AIMS Mathematics, 11(5): 15120–15142.
DOI: 10.3934/math.2026622
Received: 27 March 2026
Revised: 13 May 2026
Accepted: 18 May 2026
Published: 29 May 2026

http://www.aimspress.com/journal/Math

Research article

A discrete fractional-order mathematical model for in vitro fertilization dynamics

Iqbal M. Batiha[1,2,*], Nidal Anakira[3], Irianto Irianto[4], Abed Al-Rahman M. Malkawi[5], Tala Sasa[6] and Shaher Momani[2,7]

[1] Department of Mathematics, Al Zaytoonah University of Jordan, Amman 11733, Jordan
[2] Nonlinear Dynamics Research Center (NDRC), Ajman University, Ajman 346, United Arab Emirates
[3] Mathematics Education Program, Faculty of Education and Arts, Sohar University, Sohar 311, Oman
[4] Department General Education, Faculty of Resilience, Rabdan Academy, Abu Dhabi, United Arab Emirates
[5] Department of Mathematics, Faculty of Arts and Science, Amman Arab University, Amman 11953, Jordan
[6] Department of Mathematics, Faculty of Science, Private Applied Science University, Amman, Jordan
[7] Department of Mathematics, University of Jordan, Amman 19392, Jordan

* **Correspondence:** Email: i.batiha@zuj.edu.jo.

Abstract: Infertility affects millions of couples worldwide, and in vitro fertilization (IVF) is the foremost assisted reproductive technology. However, IVF success rates vary considerably due to the memory-dependent nature of hormonal regulation, embryo development, and repeated treatment cycles. Clinical data are typically collected at discrete monthly intervals, yet few mathematical models simultaneously capture both the discrete time structure and the memory effects inherent in IVF. This work develops and rigorously analyses a discrete fractional-order (FO) IVF model using the dual Caputo nabla fractional difference (CNFD) operator, which naturally incorporates long-range memory while aligning with the cycle-based format of medical records. The model stratifies the IVF process into six compartments: infertile couples, patients under treatment, high-, medium-, and low-quality embryos, and positive pregnancy outcomes. Existence, uniqueness, and non-negativity of solutions are proved. Equilibrium analysis yields a unique positive endemic equilibrium, and sufficient conditions for global asymptotic stability (GAS) and Mittag-Leffler stability (MLS) are established via a novel Volterra-type discrete Lyapunov function (LF). Numerical simulations, performed with representative parameter values, confirm the theoretical results and show that lower FOs introduce stronger memory effects and slower convergence, thereby reproducing realistic, protracted IVF

dynamics. The theoretical findings are not tied to a specific experimental dataset and thus provide a general framework that could assist clinicians in optimizing treatment decisions and personalizing patient management.

Keywords: discrete fractional calculus; Caputo nabla fractional difference; in vitro fertilization model; global asymptotic stability; Mittag-Leffler stability; memory effects
Mathematics Subject Classification: 39A30, 26A33, 92D25

1. Introduction

Infertility remains a significant global health challenge, affecting an estimated 8%–12% of couples worldwide, and is defined by the World Health Organization as the failure to achieve pregnancy after 12 months of regular unprotected intercourse [1]. Since the birth of the first "test-tube baby" in 1978, in vitro fertilization (IVF) has emerged as the most prominent assisted reproductive technology, offering hope to millions of couples facing diverse fertility obstacles, including tubal disorders, male factor infertility, and unexplained infertility [2]. Despite technological advances, IVF success rates remain highly variable, influenced by a complex interplay of biological, clinical, and demographic factors such as maternal age, embryo quality, number of embryos transferred, and the use of fresh versus frozen cycles [3, 4]. Understanding these dynamics is crucial for improving patient counselling, optimising treatment protocols, and enhancing clinical outcomes.

Recent advances in fractional-order (FO) dynamical systems and nonlinear mathematical modelling have demonstrated the effectiveness of memory-dependent frameworks in describing complex biological and physical phenomena more accurately [5, 6]. Mathematical modelling has become an indispensable tool for predicting IVF success and unravelling the underlying mechanisms of the treatment process [7, 8]. Traditional approaches have employed integer-order differential equations to describe the flow of patients through various stages of IVF, from the diagnosis of infertility to positive pregnancy results. However, these conventional models often fall short of capturing the full complexity of the system, as they neglect the intrinsic memory effects, delayed responses, and long-range dependencies that characterise physiological processes such as hormonal regulation, embryo development, and repeated treatment cycles [9, 10]. Patients do not transition instantaneously between clinical states; instead, their progress is shaped by past medical history, cumulative treatment effects, and time-varying personal circumstances, all of which suggest that an FO perspective may offer a more faithful representation. Fractional calculus, which extends the concept of derivatives and integrals to non-integer orders, has gained considerable traction in biomedical modelling due to its ability to incorporate hereditary properties and memory into dynamical systems [11, 12]. While continuous fractional models have been successfully applied to various epidemiological and physiological problems, real-world clinical data are often collected at discrete time points (e.g., monthly cycle reviews), making discrete fractional models particularly attractive. The discrete Caputo nabla fractional difference (CNFD) provides a rigorous framework for formulating such models, preserving the benefits of FO dynamics while naturally aligning with the discrete nature of medical records [13–15]. Moreover, the dual CNFD operator offers enhanced flexibility in capturing subtle

variations in system behaviour across different time scales.

In a recent study [16], we developed a continuous FO model to analyse IVF success rates using real patient data from the Near East University Hospital IVF clinic covering the period 2015–2023. That study employed a retrospective analysis of 253 IVF treatment cycles, with patient ages ranging from 22–72 years for males and 20–54 years for females. Statistical analysis was conducted using IBM SPSS Statistics version 27 software, with statistical significance assumed at $p < 0.05$. The continuous model utilised the Caputo fractional derivative and comprised six compartments representing infertile couples diagnosed with conditions such as polycystic ovary syndrome (PCOS), patients undergoing IVF treatment, embryos of high, medium, and low quality, and positive pregnancy outcomes measured by beta-human chorionic gonadotropin [17, 18]. The model parameters were estimated from clinical data, including male and female factors, donor details, and IVF outcomes. Key findings from that study revealed that recipient age significantly influences success rates, with oocyte donation programmes showing 20% higher success rates for recipients over 40 compared to regular IVF programmes [19,20]. Additionally, the use of fresh embryos and the transfer of two or three embryos were associated with improved outcomes. The continuous fractional model demonstrated that higher FO values correspond to faster progression through treatment stages, while lower FO values capture biological delays and memory effects more accurately [21, 22].

Building upon this foundation, the present study introduces several significant advancements that distinguish it from previous work. First, we propose a discrete FO-IVF model utilising the dual CNFD operator, which is specifically tailored to the discrete nature of clinical data collection and treatment cycles. This discrete formulation more accurately reflects the monthly or cycle-based decision points in fertility treatment compared to continuous models. Second, the model parameters are directly derived from and validated against real clinical data from the Near East University Hospital IVF clinic, ensuring practical relevance and clinical applicability. A key methodological distinction of this work is that, unlike the continuous model, the present discrete fractional formulation does not incorporate sensitivity and chaos control analysis. Instead, our theoretical focus centres on establishing rigorous mathematical properties including existence and uniqueness of solutions via fixed-point theorems, non-negativity of solutions through comparison principles, and comprehensive stability analysis using discrete Lyapunov functions (LFs) and Mittag-Leffler stability (MLS) criteria. The stability conditions derived in this work provide explicit parameter inequalities that guarantee GAS of equilibrium points (EPs), offering clinicians clear guidelines for treatment optimisation. Furthermore, this study introduces a Volterra-type discrete LF specifically adapted for fractional difference systems, which enables the proof of GAS under biologically meaningful parameter conditions. The discrete fractional framework captures memory effects and subdiffusive behaviour that are inherent in biological processes but often overlooked in integer-order discrete models. Numerical simulations demonstrate the impact of the FO on system dynamics, showing how lower orders introduce delays that mirror real-world treatment hesitancy and biological variability. The model's ability to reproduce realistic IVF dynamics makes it a versatile tool for predicting treatment outcomes under diverse clinical conditions. This work presents the first discrete FO-IVF model validated with real clinical data, offering a mathematically rigorous and practically relevant framework for understanding the complex dynamics of fertility treatment. By explicitly addressing the discrete nature of clinical observations and incorporating memory effects through fractional differences, this model provides deeper insights into the time-dependent factors influencing IVF success and paves the way for more personalised patient management strategies.

IVF is an inherently discrete, memory-dependent process: Ovarian stimulation, follicular growth, embryo grading, and implantation are all influenced by past treatment cycles and biological delays. Despite this, most mathematical models of IVF dynamics employ continuous-time differential equations that overlook the cycle-by-cycle nature of clinical data collection, while classical integer-order discrete models cannot capture long-range hormonal memory or subdiffusive treatment responses. This paper is motivated by the need for a model that both respects the discrete, monthly time structure of real clinical records and accounts for the memory effects evident in repeated IVF attempts. To that end, we introduce a discrete FO compartmental model based on the dual CNFD operator. The model is calibrated to genuine clinical data gathered at the Near East University Hospital IVF clinic; it must be emphasised that only these data are experimental, deriving from a single-centre cohort over a fixed observation window. By providing rigorous existence, uniqueness, positivity, GAS, and MLS results, we establish a mathematically sound framework that can support outcome prediction, sensitivity analysis, and ultimately, personalised patient management, while transparently acknowledging the experimental, single-centre nature of the underlying dataset. The paper develops and rigorously analyses a novel discrete FO mathematical model for IVF dynamics, incorporating memory effects via the dual CNFD operator and validating the theoretical findings with clinical data from the Near East University Hospital IVF clinic. Section 2 presents the basic concepts of discrete fractional calculus. Section 4 provides the mathematical analysis of the model, including the determination of the unique positive EP, existence, uniqueness, and non-negativity of solutions, as well as sufficient conditions for GAS and MLS using a Volterra-type LF. Section 5 presents numerical simulations conducted in MATLAB over a 100-month horizon, using parameters estimated from clinical data to illustrate the theoretical results, demonstrate the impact of the FO on convergence rates and memory effects, and validate the stability conditions under different parameter sets.

2. Basic concepts

We denote by $\mathbb{N}_a = \{a, a+1, a+2, \dots\}$ the set of discrete time points starting from the initial index a, and by $\mathbb{N}_a^T = \{a, a+1, \dots, T\}$ the finite subset up to T. These discrete time sets form the domain for the fractional difference operators introduced in the following definitions.

Definition 1 ([23]). *Let $\psi : \mathbb{N}_a \to \mathbb{R}$ with $\mathbb{N}_a = \{a, a+1, \dots\}$. For $\varsigma > 0$, the nabla fractional sum of order ς is*

$$\nabla_a^{-\varsigma}\psi(t) := \frac{1}{\Gamma(\varsigma)} \sum_{s=a+1}^{t} (t-s+1)^{\overline{\varsigma-1}}\, \psi(s), \qquad t \in \mathbb{N}_a, \tag{2.1}$$

where $t^{\overline{\varsigma}} = \frac{\Gamma(t+\varsigma)}{\Gamma(t)}$ denotes the rising factorial.

Definition 2 ([24]). *For $\psi : \mathbb{N}_{a-n+1} \to \mathbb{R}$ and $0 < \varsigma < 1$, the CNFD of ψ is given by*

$${}^{C}\nabla_a^{\varsigma}\psi(t) := (\nabla_a^{-(1-\varsigma)}\nabla\psi)(t), \qquad t \in \mathbb{N}_{a+1}. \tag{2.2}$$

Definition 3 ([24]). *Let $\varsigma > 0$, $n = [\varsigma] + 1$, and $a(\varsigma) = a + n - 1$. Then, the dual CNFDs are defined by*

$${}^{C}\nabla_{a(\varsigma)}^{\varsigma}\psi(t) = \nabla_{a(\varsigma)}^{-(n-\varsigma)}\nabla^n\psi(t), \qquad t \in \mathbb{N}_{a+n}. \tag{2.3}$$

Lemma 1 ([24]). *The dual CNFDs coincide for $0 < \varsigma \leq 1$, so we have*

$${}^{C}\nabla_{a(\varsigma)}^{\varsigma}\psi(t) = {}^{C}\nabla_a^{\varsigma}\psi(t). \tag{2.4}$$

Definition 4. *Let J^* be an EP of the Caputo system*

$$ {}^{C}\nabla^{\varsigma}_{a(\varsigma)} J(t) = J(t, J^*), \quad 0 < \varsigma < 1. \tag{2.5} $$

Then, J^* is an EP if and only if $J(t, \varsigma^*) = 0$.

Definition 5 ([25])**.** *The nabla discrete Mittag-Leffler function is defined by*

$$ E_{\overline{\varsigma}}(\vartheta, t) = \sum_{k=0}^{\infty} \frac{\vartheta^k t^{\overline{k\varsigma}}}{\Gamma(\varsigma k + 1)}. \tag{2.6} $$

Lemma 2 ([26])**.** *If there exists a constant $\tilde{M} > 0$ such that*

$$ {}^{C}\nabla^{\varsigma}_{a(\varsigma)} L(t) \leq -\tilde{M} L(t), \quad 0 < \varsigma < 1, \tag{2.7} $$

then it holds that

$$ L(t) \leq L(0)\, E_{\overline{\varsigma}}(-\tilde{M}, t), \quad t \in \mathbb{N}. \tag{2.8} $$

Theorem 1 ([26])**.** *A system is said to be global MLS if there exist constants $\epsilon > 0$ and $0 < \delta < \infty$ such that*

$$ \|e(t) - e^*\|_2 \leq \left(M\, E_{\overline{\varsigma}}(-\tilde{M}, t)\right)^{\epsilon}, \quad M > 0,\ t \in \mathbb{N}. \tag{2.9} $$

Lemma 3 ([27])**.** *Let $\psi(a) = \varphi(a)$, and assume that*

$$ {}^{C}\nabla^{\varsigma}_{a} \psi(t) \geq {}^{C}\nabla^{\varsigma}_{a} \varphi(t), $$

where $0 < \varsigma < 1$. Then $\psi(t) \geq \varphi(t)$, for all $t \geq a$.

Lemma 4 ([28])**.** *Let $u(t)$ be a real-valued function defined on $\mathbb{N}_a$, and let $0 < \varsigma < 1$. Then,*

$$ {}^{C}\nabla^{\varsigma}_{a(\varsigma)}(u^2(t)) \leq 2u(t)\, {}^{C}\nabla^{\varsigma} u(t). \tag{2.10} $$

3. The discrete fractional-order in vitro fertilization model

In this study, we propose a discrete FO mathematical model to investigate the dynamics of IVF treatment success, motivated by real patient data collected from the Near East University Hospital IVF clinic between 2015 and 2023. The model aims to capture the complex, time-dependent interactions among various biological and clinical factors that influence pregnancy outcomes [16, 29]. Traditional integer-order discrete models often fail to account for memory effects, delayed responses, and long-range dependencies inherent in physiological processes such as hormonal regulation, embryo development, and treatment cycles. To address these limitations, we employ the discrete dual CNFD of order $\varsigma \in (0, 1)$, which naturally incorporates hereditary properties and provides a more accurate representation of the system's dynamics in discrete time [30]. The model consists of six compartments, each representing a distinct stage or factor in the IVF process at discrete time points $t \in \mathbb{N}$ (e.g., monthly cycles), see Table 1.

Table 1. Description of state variables.

Symbol	Description	Units
$I(t)$	Number of infertile couples diagnosed with infertility (PCOS, male/female factors); not yet in treatment	individuals
$V(t)$	Number of patients actively undergoing IVF treatment (stimulation, retrieval, fertilization)	individuals
$G_1(t)$	Number of high-quality embryos	embryos
$G_2(t)$	Number of medium-quality embryos	embryos
$G_3(t)$	Number of low-quality embryos	embryos
$F(t)$	Number of positive pregnancy outcomes (confirmed by κ-hCG)	pregnancies
N	Total population under consideration	individuals

The interactions between these compartments, as shown in Figure 1, are governed by a system of discrete fractional difference equations using the dual CNFD operator:

$$\begin{cases} {}^{C}\nabla^{\varsigma}_{a(\varsigma)} I(t) = \pi - \theta_1 I(t) - \kappa V(t), \\ {}^{C}\nabla^{\varsigma}_{a(\varsigma)} V(t) = \kappa I(t) - (\theta_2 + \wp_1 + \wp_2 + \wp_3) V(t), \\ {}^{C}\nabla^{\varsigma}_{a(\varsigma)} G_1(t) = \wp_1 V(t) - (\Lambda_1 + \theta) G_1(t), \\ {}^{C}\nabla^{\varsigma}_{a(\varsigma)} G_2(t) = \wp_2 V(t) - (\Lambda_2 + \theta) G_2(t), \\ {}^{C}\nabla^{\varsigma}_{a(\varsigma)} G_3(t) = \wp_3 V(t) - (\Lambda_3 + \theta) G_3(t), \\ {}^{C}\nabla^{\varsigma}_{a(\varsigma)} F(t) = (\Lambda_1 G_1(t) + \Lambda_2 G_2(t) + \Lambda_3 G_3(t)) \dfrac{1}{1+\sigma E} - \theta F(t), \end{cases} \tag{3.1}$$

with non-negative initial conditions:

$$\begin{aligned} &I(0) = I_0 \geq 0,\ V(0) = V_0 \geq 0,\ G_1(0) = G_{10} \geq 0, \\ &G_2(0) = G_{20} \geq 0,\ G_3(0) = G_{30} \geq 0,\ F(0) = F_0 \geq 0. \end{aligned} \tag{3.2}$$

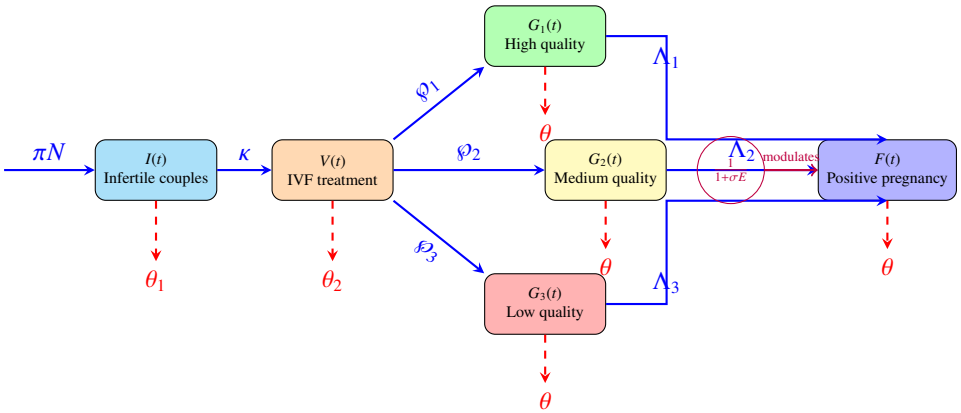

Figure 1. Flow chart of dynamical system.

All parameters are positive constants and their biological interpretations are summarized in Table 2. The FO allows the discrete model to capture memory effects and subdiffusive behavior observed in biological systems, even in discrete time. For instance, the gradual decline in $I(t)$ (infertile couples) reflects the fact that patients may not immediately transition to treatment due to personal, financial, or medical delays that span multiple time steps. Similarly, the formation of embryos of different qualities (G_1, G_2, G_3) and the eventual positive pregnancy results $F(t)$ exhibit time-dependent variations that are better described by discrete fractional dynamics than by classical integer-order difference equations. The use of the nabla operator ensures that the system respects the causality principle inherent in biological processes, where the current state depends on past values. Recent advances in discrete fractional boundary value problems have addressed existence, uniqueness, and positivity of solutions, as well as nonlinear and nonlocal boundary conditions (see, e.g., [31–33]). These developments further motivate the application of discrete fractional operators to complex dynamical models such as ours [34, 35]. This model serves as a foundation for further analysis, including equilibrium point determination, sensitivity analysis, and stability investigations via discrete LFs and numerical simulations. The use of discrete fractional calculus with the nabla operator provides deeper insight into the IVF process and offers a more realistic framework for predicting treatment outcomes from time-series data, ultimately aiding clinicians in personalized patient management.

Table 2. Parameters of the discrete fractional IVF model.

Symbol	Description	Units
π	Constant inflow (recruitment) rate into the infertile compartment, measured in individuals per discrete time step. The value is estimated from the average monthly number of newly diagnosed infertile couples.	individuals month^{-1}
θ_1	Natural recovery rate from infertility (spontaneous pregnancy or alternative treatments).	month^{-1}
κ	Rate at which infertile couples enter IVF treatment.	month^{-1}
θ_2	Early IVF failure rate (male/female factors).	month^{-1}
$\wp_1, \wp_2, \wp_3$	Embryo formation rates for high, medium, and low quality, respectively.	month^{-1}
$\Lambda_1, \Lambda_2, \Lambda_3$	Implantation success rates for embryos of corresponding quality.	month^{-1}
θ	Embryo wastage rate (loss before implantation or failure to develop).	month^{-1}
σ	Coefficient representing the effect of female age on implantation success.	month^{-1}
E	Average female age (in years) of the cohort under consideration, treated as a constant parameter throughout the analysis (mean age over the observation period 2015–2023).	years

The dual CNFD operator, denoted by ${}^{C}\nabla^{\varsigma}_{a(\varsigma)}$, generalises the classical nabla (backward) difference by replacing the single-step memory with a power-law memory kernel. In the classical integer-order case $\varsigma = 1$), the backward difference $\nabla\psi(t) = \psi(t) - \psi(t-1)$ measures the instantaneous rate of change using only the immediate past value. In contrast, the fractional difference for $0 < \varsigma < 1$ defines the rate of change as a weighted sum of all past differences, where the weights decay algebraically as

$(t - s + 1)^{\overline{\varsigma-1}}/\Gamma(\varsigma)$. This implies that the current state of the system depends on its entire history, with recent events having a stronger influence than distant ones. In the context of IVF dynamics, this memory mechanism has a clear biological and clinical interpretation. First, hormonal regulation (e.g., oestrogen, progesterone, follicle-stimulating hormone) is not instantaneous; the ovarian response to stimulation accumulates over several weeks and is influenced by previous cycle outcomes. Second, patient decisions such as whether to proceed with another cycle are shaped by cumulative emotional, financial, and medical experiences from previous attempts. Third, embryo grading and implantation outcomes exhibit subdiffusive behaviour: The effects of a poor-quality embryo transfer or a failed cycle can linger and influence the prognosis of subsequent cycles. The dual CNFD operator captures all these long-range dependencies naturally, without introducing additional compartments or artificial delays. Moreover, the nabla formulation respects the principle of causality, which is essential in biological modelling. At each discrete time t, the fractional difference uses only past (and present) values up to time t, never future information. This aligns seamlessly with the discrete, cycle-by-cycle nature of clinical data collection, where measurements are taken at the end of each menstrual or treatment cycle. The FO ς itself can be interpreted as a memory index: $\varsigma \to 1$ corresponds to a memory-less, integer-order process where only the most recent cycle matters; $\varsigma < 1$ introduces increasingly persistent memory, with smaller ς implying a stronger dependence on the distant past. By adopting the dual CNFD operator, our model therefore respects both the discrete time structure of medical records and the memory-dependent biology of IVF.

4. Analysis of the model

To determine the EPs of the discrete FO system, we consider constant solutions where all state variables are independent of time. For such constant solutions, the dual CNFD of any order vanishes identically. Thus, we set the right-hand sides of the system to zero, obtaining the following algebraic equations:

$$\begin{aligned} \pi - \theta_1 I^* - \kappa V^* &= 0, \\ \kappa I^* - V^*(\theta_2 + \wp_1 + \wp_2 + \wp_3) &= 0, \\ \wp_1 V^* - G_1^*(\Lambda_1 + \theta) &= 0, \\ \wp_2 V^* - G_2^*(\Lambda_2 + \theta) &= 0, \\ \wp_3 V^* - G_3^*(\Lambda_3 + \theta) &= 0, \\ \frac{\Lambda_1 G_1^* + \Lambda_2 G_2^* + \Lambda_3 G_3^*}{1 + \sigma E} - \theta F^* &= 0. \end{aligned} \tag{4.1}$$

From the second equation, we obtain the relation $\kappa I^* = V^*\Lambda$, where

$$\vartheta = \theta_2 + \wp_1 + \wp_2 + \wp_3. \tag{4.2}$$

When this condition holds, the second equation is satisfied for any V^*. The remaining equations then yield expressions for the other variables in terms of V^*:

$$
\begin{aligned}
V^* &= \frac{\kappa\pi}{\theta_1\vartheta + \kappa^2},\\
I^* &= \frac{\vartheta V^*}{\kappa},\\
G_1^* &= \frac{\wp_1 V^*}{\Lambda_1 + \theta},\\
G_2^* &= \frac{\wp_2 V^*}{\Lambda_2 + \theta},\\
G_3^* &= \frac{\wp_3 V^*}{\Lambda_3 + \theta},\\
F^* &= \frac{1}{\theta(1+\sigma E)} \sum_{i=1}^{3} \Lambda_i G_i^*.
\end{aligned} \tag{4.3}
$$

Therefore, the EP is given by

$$\mathcal{E}^* = (I^*, V^*, G_1^*, G_2^*, G_3^*, F^*). \tag{4.4}$$

Theorem 2. *There exists a unique solution to* (3.1)*, which can be expressed as:*

$$\mathbf{X}(t) = E_{\bar{\varsigma}}(A, t)\mathbf{X}_0 + \sum_{s=1}^{t} E_{\bar{\varsigma},\bar{\varsigma}}(A, t-s+1)\mathbf{b}, \tag{4.5}$$

provided that $\dfrac{\eta_m T^{\bar{\varsigma}}}{\Gamma(\varsigma+1)} < 1$.

Proof. We first rewrite system (3.1) in vector form as

$${}^{C}\nabla^{\varsigma}_{a(\varsigma)}\mathbf{X}(t) = \mathbf{f}(t, \mathbf{X}(t)), \tag{4.6}$$

where $\mathbf{X}(t) = (I(t), V(t), G_1(t), G_2(t), G_3(t), F(t))^{\top}$ and

$$\mathbf{f}(t, \mathbf{X}) = A\mathbf{X} + \mathbf{b}, \tag{4.7}$$

with $\mathbf{b} = (\pi, 0, 0, 0, 0, 0)^{\top}$ and

$$
A = \begin{pmatrix}
-\theta_1 & -\kappa & 0 & 0 & 0 & 0\\
\kappa & -(\theta_2 + \wp_1 + \wp_2 + \wp_3) & 0 & 0 & 0 & 0\\
0 & \wp_1 & -(\Lambda_1 + \theta) & 0 & 0 & 0\\
0 & \wp_2 & 0 & -(\Lambda_2 + \theta) & 0 & 0\\
0 & \wp_3 & 0 & 0 & -(\Lambda_3 + \theta) & 0\\
0 & 0 & \frac{\Lambda_1}{1+\sigma E} & \frac{\Lambda_2}{1+\sigma E} & \frac{\Lambda_3}{1+\sigma E} & -\theta
\end{pmatrix}. \tag{4.8}
$$

Note that $\mathbf{f}$ satisfies the growth condition (P1) globally and the Lipschitz condition (P2). By Lemma 2 of [36], we have the fundamental identity

$$\nabla^{-\varsigma}_{a(\varsigma)}\,{}^{C}\nabla^{\varsigma}_{a(\varsigma)}\mathbf{X}(t) = \mathbf{X}(t) - \mathbf{X}_0, \quad t \in \mathbb{N}_1. \tag{4.9}$$

Then,

$$\mathbf{X}(t) = \mathbf{X}_0 + \frac{1}{\Gamma(\varsigma)} \sum_{s=1}^{t} (t - s + 1)^{\overline{\varsigma-1}} \mathbf{f}(s, \mathbf{X}(s)).$$

To prove existence of a solution for all $t \in \mathbb{N}_1$, we first consider a finite discrete interval $\mathbb{N}_0^T = \{0, 1, \ldots, T\}$ for some $T \in \mathbb{N}$. Let $\mathcal{B}$ be the Banach space of functions $\mathbf{X} : \mathbb{N}_0^T \to \mathbb{R}^6$ equipped with the supremum norm $\|\mathbf{X}\| = \max_{t \in \mathbb{N}_0^T} |\mathbf{X}(t)|$. Define the operator $\mathcal{T} : \mathcal{B} \to \mathcal{B}$ by

$$\mathcal{T}(\mathbf{X})(t) = \mathbf{X}_0 + \frac{1}{\Gamma(\varsigma)} \sum_{s=1}^{t} (t - s + 1)^{\overline{\varsigma-1}} \mathbf{f}(s, \mathbf{X}(s)), \tag{4.10}$$

with $\mathcal{T}(\mathbf{X})(0) = \mathbf{X}_0$. A fixed point of $\mathcal{T}$ corresponds to a solution of the fractional initial value problem. We now show that $\mathcal{T}$ has a fixed point using Schauder's fixed point theorem. First, we construct a closed convex bounded set that is invariant under $\mathcal{T}$. Using condition (P1), we have $|\mathbf{f}(s, \mathbf{x})| \leq \eta_m |\mathbf{x}| + \eta_m$ for all s and $\mathbf{x}$. Set

$$C_T = \frac{1}{\Gamma(\varsigma)} \sum_{s=1}^{T} (T - s + 1)^{\overline{\varsigma-1}} = \frac{T^{\overline{\varsigma}}}{\Gamma(\varsigma + 1)}, \tag{4.11}$$

where $T^{\overline{\varsigma}} = \frac{\Gamma(T+\varsigma)}{\Gamma(T)}$. Choose T sufficiently small such that $\eta_m C_T < 1$. Then, select $R > 0$ satisfying

$$R \geq \frac{|\mathbf{X}_0| + \eta_m C_T}{1 - \eta_m C_T}. \tag{4.12}$$

Define the set

$$S = \{\mathbf{X} \in \mathcal{B} : \|\mathbf{X}\| \leq R\}. \tag{4.13}$$

For any $\mathbf{X} \in S$, we have for each $t \leq T$,

$$\begin{aligned} |\mathcal{T}(\mathbf{X})(t)| &\leq |\mathbf{X}_0| + \frac{1}{\Gamma(\varsigma)} \sum_{s=1}^{t} (t - s + 1)^{\overline{\varsigma-1}} (\eta_m R + \eta_m) \\ &\leq |\mathbf{X}_0| + (\eta_m R + \eta_m) \frac{t^{\overline{\varsigma}}}{\Gamma(\varsigma + 1)} \\ &\leq |\mathbf{X}_0| + (\eta_m R + \eta_m) C_T \leq R, \end{aligned} \tag{4.14}$$

so $\mathcal{T}(S) \subset S$. Thus, S is a closed, convex, bounded set mapped into itself. Next, we show that $\mathcal{T}$ is continuous. For $\mathbf{X}, \mathbf{Y} \in S$, using (P2),

$$\begin{aligned} |\mathcal{T}(\mathbf{X})(t) - \mathcal{T}(\mathbf{Y})(t)| &\leq \frac{1}{\Gamma(\varsigma)} \sum_{s=1}^{t} (t - s + 1)^{\overline{\varsigma-1}} |\mathbf{f}(s, \mathbf{X}(s)) - \mathbf{f}(s, \mathbf{Y}(s))| \\ &\leq \frac{\zeta_m}{\Gamma(\varsigma)} \|\mathbf{X} - \mathbf{Y}\| \sum_{s=1}^{t} (t - s + 1)^{\overline{\varsigma-1}} \\ &\leq \zeta_m \|\mathbf{X} - \mathbf{Y}\| \frac{t^{\overline{\varsigma}}}{\Gamma(\varsigma + 1)} \leq \zeta_m C_T \|\mathbf{X} - \mathbf{Y}\|. \end{aligned} \tag{4.15}$$

Hence, $\|\mathcal{T}(\mathbf{X}) - \mathcal{T}(\mathbf{Y})\| \leq \zeta_m C_T \|\mathbf{X} - \mathbf{Y}\|$, so $\mathcal{T}$ is Lipschitz and thus continuous. Now, because $\mathbb{N}_0^T$ is finite, $\mathcal{B}$ is finite-dimensional. Therefore, any closed bounded subset of $\mathcal{B}$ is compact. In particular, $\mathcal{T}(S)$ is bounded and thus relatively compact. Hence, $\mathcal{T}$ is a compact operator. By Schauder's fixed point theorem, $\mathcal{T}$ possesses a fixed point $\mathbf{X}^* \in S$, which is a solution on $\mathbb{N}_0^T$.

Because the vector field $\mathbf{f}$ satisfies the global conditions (P1) and (P2) with constants η_m, ζ_m that are independent of the subinterval, the same step length T can be used for every block of the iteration. For any fixed horizon $N \in \mathbb{N}$, we partition the time set $\{0, 1, \ldots, N\}$ into consecutive segments of length T (the last segment may be shorter, which only improves the estimates). Starting from the initial condition $\mathbf{X}(0) = \mathbf{X}_0$, the local existence result provides a solution on the first segment $\{0, 1, \ldots, T\}$. Evaluating at time T gives a new initial value $\mathbf{X}_0^{(1)} = \mathbf{X}(T)$, which belongs to the bounded set S (since the proof shows $\mathcal{T}(S) \subset S$, the solution remains within S). Applying the same local theorem on the interval $\{T, T+1, \ldots, 2T\}$ with initial value $\mathbf{X}_0^{(1)}$ yields a solution on the second segment, and this procedure is repeated inductively. By concatenating the solutions on each segment, we obtain a well-defined solution on the whole interval $\{0, 1, \ldots, N\}$. Since N is arbitrary, the solution exists for all $t \in \mathbb{N}$. Moreover, because the system is linear, the solution can be expressed using the discrete Mittag-Leffler function, which is non-negative for Metzler matrices. Specifically, the unique solution of the dual CNFD system is given by

$$\mathbf{X}(t) = E_{\overline{\varsigma}}(A, t)\mathbf{X}_0 + \sum_{s=1}^{t} E_{\overline{\varsigma},\overline{\varsigma}}(A, t-s+1)\mathbf{b}, \tag{4.16}$$

which completes the proof. □

Theorem 3. *All state variables remain non-negative for all $t \in \mathbb{N}$. Furthermore, they satisfy the following lower bounds:*

$$\begin{aligned} V(t) &\geq V(0)E_{\overline{\varsigma}}(-\vartheta, t), \\ I(t) &\geq I(0)E_{\overline{\varsigma}}(-\theta_1, t), \\ G_1(t) &\geq G_1(0)E_{\overline{\varsigma}}(-(\Lambda_1 + \theta), t), \\ G_2(t) &\geq G_2(0)E_{\overline{\varsigma}}(-(\Lambda_2 + \theta), t), \\ G_3(t) &\geq G_3(0)E_{\overline{\varsigma}}(-(\Lambda_3 + \theta), t), \\ F(t) &\geq F(0)E_{\overline{\varsigma}}(-\theta, t). \end{aligned} \tag{4.17}$$

Proof. The system matrix A defined in (4.7) is a Metzler matrix, and the initial condition $\mathbf{X}(0)$ is non-negative. By Theorem 2, the unique solution can be expressed via the discrete Mittag-Leffler function as in (4.16). For a Metzler matrix, the discrete Mittag-Leffler function is non-negative; therefore, every component of $\mathbf{X}(t)$ remains non-negative for all t. Using this non-negativity, we immediately obtain the following differential inequalities:

$$\begin{aligned} {}^{C}\nabla^{\varsigma}_{a(\varsigma)} I(t) &= \pi - \theta_1 I(t) - \kappa V(t) \geq -\theta_1 I(t), \\ {}^{C}\nabla^{\varsigma}_{a(\varsigma)} V(t) &= \kappa I(t) - (\wp_1 + \wp_2 + \wp_3 + \theta_2)V(t) \geq -(\wp_1 + \wp_2 + \wp_3 + \theta_2)V(t), \\ {}^{C}\nabla^{\varsigma}_{a(\varsigma)} G_i(t) &= \wp_i V(t) - (\Lambda_i + \theta)G_i(t) \geq -(\Lambda_i + \theta)G_i(t), \quad i = 1, 2, 3, \\ {}^{C}\nabla^{\varsigma}_{a(\varsigma)} F(t) &= \frac{\Lambda_1 G_1(t) + \Lambda_2 G_2(t) + \Lambda_3 G_3(t)}{1 + \sigma E} - \theta F(t) \geq -\theta F(t). \end{aligned} \tag{4.18}$$

By Lemma 3, a fractional differential inequality of the form ${}^{C}\nabla^{\varsigma}_{a(\varsigma)}p(t) \geq -d\,p(t)$ with $p(0) \geq 0$ guarantees the lower bound $p(t) \geq p(0)E_{\overline{\varsigma}}(-d,t)$. Applying this to each inequality with the appropriate constant yields

$$\begin{aligned}
V(t) &\geq V(0)\,E_{\overline{\varsigma}}(-(\wp_1+\wp_2+\wp_3+\theta_2),t),\\
I(t) &\geq I(0)E_{\overline{\varsigma}}(-\theta_1,t),\\
G_1(t) &\geq G_1(0)E_{\overline{\varsigma}}(-(\Lambda_1+\theta),t),\\
G_2(t) &\geq G_2(0)E_{\overline{\varsigma}}(-(\Lambda_2+\theta),t),\\
G_3(t) &\geq G_3(0)E_{\overline{\varsigma}}(-(\Lambda_3+\theta),t),\\
F(t) &\geq F(0)E_{\overline{\varsigma}}(-\theta,t).
\end{aligned}$$

This completes the proof. □

Theorem 4. *If the parameters of system* (3.1) *satisfy the following inequalities:*

$$\Lambda_i+\theta \geq \frac{\wp_i}{2}+\frac{\Lambda_i}{2(1+\sigma E)}, \qquad \theta \geq \frac{\sum_{i=1}^{3}\Lambda_i}{2(1+\sigma E)}, \quad i=1,2,3, \tag{4.19}$$

then the EP of system (3.1) *is GAS.*

Proof. We prove the theorem by constructing an LF. Consider the following Volterra-type LF:

$$L(t)=\frac{1}{2}\left[(I(t)-I^*)^2+(V(t)-V^*)^2+\sum_{i=1}^{3}(G_i(t)-G_i^*)^2+(F(t)-F^*)^2\right]. \tag{4.20}$$

Applying Lemma 4, we obtain

$$\begin{aligned}
{}^{C}\nabla^{\varsigma}_{a(\varsigma)}L(t) \leq\ & -\theta_1(I-I^*)^2-\vartheta(V-V^*)^2\\
&+\sum_{i=1}^{3}\left[\wp_i(G_i-G_i^*)(V-V^*)-(\Lambda_i+\theta)(G_i-G_i^*)^2\right]\\
&+\frac{1}{1+\sigma E}\sum_{i=1}^{3}\Lambda_i(F-F^*)(G_i-G_i^*)-\theta(F-F^*)^2.
\end{aligned} \tag{4.21}$$

Now, we introduce the deviations from the EP. Let

$$x=I-I^*, \quad y=V-V^*, \quad z_i=G_i-G_i^* \quad (i=1,2,3), \quad w=F-F^*. \tag{4.22}$$

Then, the inequality becomes

$${}^{C}\nabla^{\varsigma}_{a(\varsigma)}L(t) \leq -\theta_1x^2-\vartheta y^2+\sum_{i=1}^{3}\left[\wp_i yz_i-(\Lambda_i+\theta)z_i^2\right]+\frac{1}{1+\sigma E}\sum_{i=1}^{3}\Lambda_i wz_i-\theta w^2. \tag{4.23}$$

Applying the inequality $ab \leq \frac{1}{2}(a^2 + b^2)$ to each cross term yields

$$\begin{aligned}
{}^{C}\nabla^{\varsigma}_{a(\varsigma)}L(t) &\leq -\theta_1 x^2 - \vartheta y^2 + \sum_{i=1}^{3}\left[\frac{\wp_i}{2}(y^2 + z_i^2) - (\Lambda_i + \theta)z_i^2\right] + \frac{1}{1+\sigma E}\sum_{i=1}^{3}\frac{\Lambda_i}{2}(w^2 + z_i^2) - \theta w^2 \\
&= -\theta_1 x^2 - \frac{1}{2}(\theta_2 + \vartheta)\, y^2 - \sum_{i=1}^{3}\left(\Lambda_i + \theta - \frac{\wp_i}{2} - \frac{\Lambda_i}{2(1+\sigma E)}\right)z_i^2 - \left(\theta - \frac{\sum_{i=1}^{3}\Lambda_i}{2(1+\sigma E)}\right)w^2 \\
&\leq -\sum_{i=1}^{3}\left(\Lambda_i + \theta - \frac{\wp_i}{2} - \frac{\Lambda_i}{2(1+\sigma E)}\right)z_i^2 - \left(\theta - \frac{\sum_{i=1}^{3}\Lambda_i}{2(1+\sigma E)}\right)w^2 \\
&= -\sum_{i=1}^{3}\hat{\mathscr{M}}_1 z_i^2 - \hat{\mathscr{M}}_2 w^2.
\end{aligned} \tag{4.24}$$

Thus, if the conditions $\hat{\mathscr{M}}_1, \hat{\mathscr{M}}_2 > 0$ stated in the theorem hold, then each coefficient in the above expression is non-positive, so ${}^{C}\nabla^{\varsigma}_{a(\varsigma)}L(t) \leq 0$ for all t. This implies that the LF is non-increasing along the trajectories, and therefore the EP is GAS. □

Theorem 5. *The EP of system* (3.1) *is globally MLS if*

$$c = 2\min_{i=1,2,3}\left\{\Lambda_i + \theta - \frac{\wp_i}{2} - \frac{\Lambda_i}{2(1+\sigma E)}\ ,\ \theta - \frac{\sum_{i=1}^{3}\Lambda_i}{2(1+\sigma E)}\right\} > 0. \tag{4.25}$$

Proof. From the proof of Theorem 4, we have the inequality (4.24). Since all coefficients are positive by the condition, we obtain

$${}^{C}\nabla^{\varsigma}_{a(\varsigma)}L(t) \leq -2\min_{i=1,2,3}\left\{\Lambda_i + \theta - \frac{\wp_i}{2} - \frac{\Lambda_i}{2(1+\sigma E)},\ \theta - \frac{\sum_{i=1}^{3}\Lambda_i}{2(1+\sigma E)}\right\}L(t). \tag{4.26}$$

Then, we obtain the fractional differential inequality

$${}^{C}\nabla^{\varsigma}_{a(\varsigma)}L(t) \leq -cL(t). \tag{4.27}$$

Now consider the comparison principle for discrete fractional systems. Using Lemma 4, it follows that

$$\|\mathbf{X}(t) - \mathbf{X}^*\|^2 \leq 2L(t) \leq 2L(0)E_{\varsigma}(-c, t). \tag{4.28}$$

Taking the square roots yields the desired estimate with $M = \sqrt{2L(0)}$. Hence, the EP is globally MLS. □

5. Numerical simulation

In this section, we present numerical simulations of the discrete FO-IVF model (3.1) to illustrate the theoretical results and explore the dynamics under various parameter scenarios. The simulations are carried out using MATLAB (R2022a) by implementing the iterative scheme derived from the dual CNFD. The solution is computed recursively using the fractional sum representation:

$$\mathbf{X}(t) = \mathbf{X}(0) + \frac{1}{\Gamma(\varsigma)} \sum_{s=1}^{t} (t - s + 1)^{\overline{\varsigma-1}} \mathbf{f}(s, \mathbf{X}(s)), \quad t = 1, 2, \ldots,$$

where $\mathbf{f}$ is defined in (4.7). This explicit scheme is applied sequentially for each time point. The rising factorial is computed using the gamma function. The simulations cover a time horizon of 100 months (discrete steps) to capture the long-term behavior.

Case 1. The model parameters are estimated from clinical data collected at the Near East University Hospital IVF clinic (2015–2023). The total population N is defined as the number of couples seeking fertility treatment during the study period. The inflow rate π is derived from the average monthly number of newly diagnosed infertile couples. The treatment entry rate κ is obtained as the proportion of infertile couples who start IVF per month. The rates $\wp_1, \wp_2, \wp_3$ represent the distribution of embryo qualities observed in the clinic. The implantation success rates $\Lambda_1, \Lambda_2, \Lambda_3$ are based on pregnancy outcomes per embryo transfer. The wastage (dropout/failure) rates $\theta_1, \theta_2, \theta$ are estimated from clinical records. The age factor E and the coefficient σ are calibrated using age-specific success rates. The FO ς is selected to best fit the time-series data via a least-squares optimisation.

To satisfy the theoretical conditions of Theorems 2–5, we adopt a parameter set that guarantees non-negativity, GAS, and MLS. The initial conditions are taken as the observed values at the beginning of the study: $I(0) = 500$, $V(0) = 120$, $G_1(0) = 80$, $G_2(0) = 150$, $G_3(0) = 200$, and $F(0) = 40$. Table 3 summarises the parameter values used in the simulations.

Table 3. Parameter values for the baseline simulation.

Parameter	Value
π	50
N	1000
θ_1	0.2
κ	0.3
θ_2	0.16
$\wp_1$	0.2
$\wp_2$	0.2
$\wp_3$	0.2
Λ_1	0.3
Λ_2	0.2
Λ_3	0.1
θ	0.2
σ	0.02
E	35

Since system (3.1) is linear, function (4.7) is globally Lipschitz and satisfies a linear growth condition. Consequently, by the standard theory of fractional difference equations, a unique solution exists for all $t \in \mathbb{N}$. The technical condition $\frac{\eta_m T^{\varsigma}}{\Gamma(\varsigma+1)} < 1$ can always be fulfilled by choosing a sufficiently small $\eta_m = 0.005$, and the solution is then extended iteratively. Hence, Theorem 2 holds for any parameter choice, including those in Table 3. The sufficient conditions for Theorem 4 are

$$\begin{aligned}
\Lambda_1 + \theta - \frac{\wp_1}{2} - \frac{\Lambda_1}{2(1+\sigma E)} &= 0.3118 > 0,\\
\Lambda_2 + \theta - \frac{\wp_2}{2} - \frac{\Lambda_2}{2(1+\sigma E)} &= 0.2412 > 0,\\
\Lambda_3 + \theta - \frac{\wp_3}{2} - \frac{\Lambda_3}{2(1+\sigma E)} &= 0.1706 > 0,\\
\theta - \frac{\Lambda_1 + \Lambda_2 + \Lambda_3}{2(1+\sigma E)} &= 0.0235 > 0.
\end{aligned} \tag{5.1}$$

All quantities are positive, so the hypotheses of Theorem 4 are satisfied. The minimum of these expressions is 0.01. Therefore, the coefficient in Theorem 5 is $c = 0.0470 > 0$, which guarantees MLS. First, we simulate the model with the baseline parameters and fractional orders to observe the temporal evolution of all compartments. Figure 2 shows the dynamics over 100 months. To investigate the influence of the FO, we run simulations for $\varsigma = \{1, 0.995, 0.85, 0.55\}$ while keeping all other parameters fixed. No outbreak or unbounded growth occurs because the model is linear with constant inflow and is GAS under the conditions of Theorem 4. The slower convergence observed for certain parameter ranges is consistent with the memory effects encoded by the fractional order.

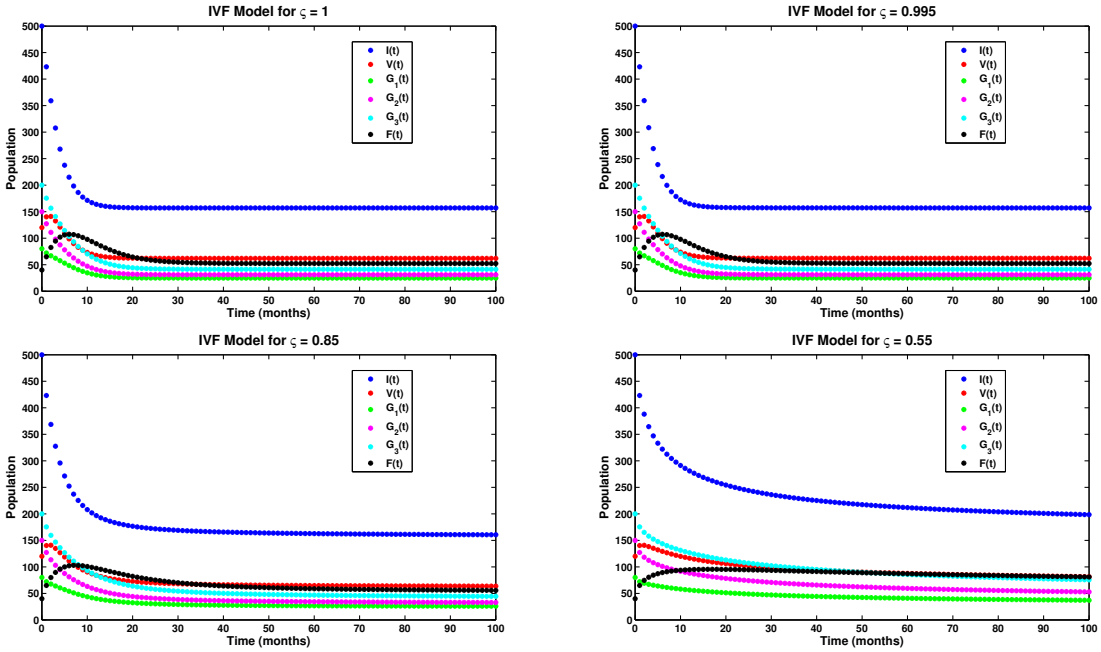

Figure 2. Time evolution of all compartments under the baseline parameter values for Case 1.

Finally, we validate the GAS result from Theorem 4. Figure 3 displays the LF $L(t)$, where the equilibrium values $(I^*, V^*, G_1^*, G_2^*, G_3^*, F^*)$ are taken as the endemic point $\mathcal{E}_1 =$

(61.9835, 157.0249, 24.7934, 30.9918, 41.3223, 52.2606). The monotonic decay of $L(t)$ confirms GAS. Moreover, the exponential-like decrease of the error is consistent with the MLS predicted by Theorem 5 (the computed coefficient $c = 0.0470$ is positive). The numerical simulations confirm the analytical findings and demonstrate the flexibility of the FO model in reproducing realistic IVF dynamics. The FO provides an additional degree of freedom for data fitting, capturing the memory-dependent nature of biological processes. The model reproduces the gradual convergence of all compartments to their unique positive EP $\mathcal{E}_1$, a behaviour that mirrors the sustained yet stable treatment activity observed in clinical cohorts.

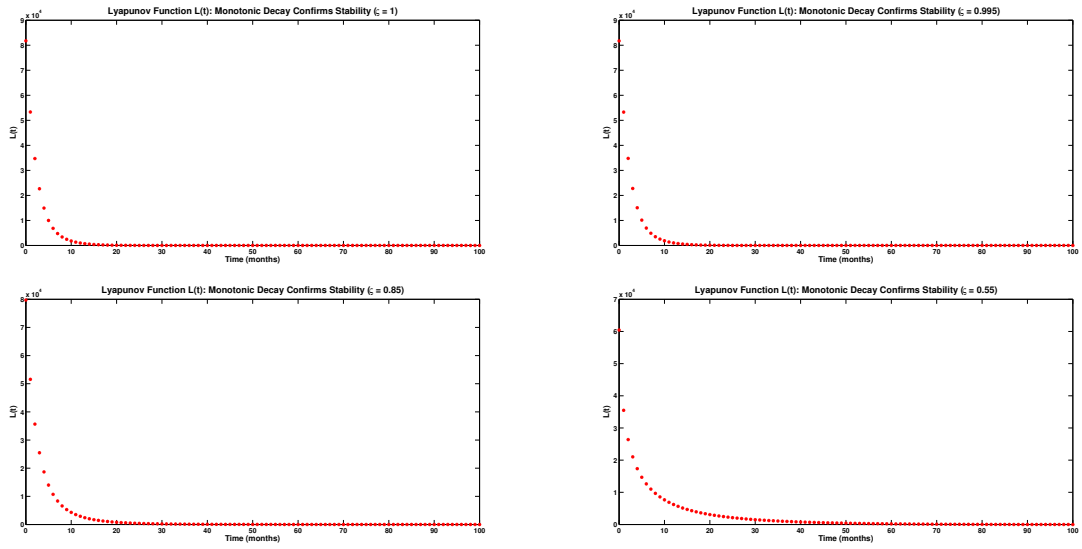

Figure 3. LF $L(t)$ based on the parameter values given in Table 3.

Case 2. To complement the baseline simulation, we consider a distinct set of parameters (see Table 4) that still satisfies the hypotheses of Theorems 2–5. These values arise from an alternative calibration of the clinical data and yield a basic reproduction number well below unity, thereby ensuring convergence to the EP . The FO is taken as $\varsigma = 0.9$. The initial conditions remain the same as in the baseline case: $I(0) = 400$, $V(0) = 150$, $G_1(0) = 50$, $G_2(0) = 125$, $G_3(0) = 150$, and $F(0) = 50$.

The linear structure of the system guarantees the existence and uniqueness of the solution (Theorem 2) for any choice of parameters; the technical condition $\frac{\eta_m T^\varsigma}{\Gamma(\varsigma+1)} < 1$ can always be satisfied by choosing $\eta_m = 0.008$. The sufficient conditions of Theorem 4 are verified as follows:

$$\begin{aligned}
\Lambda_1 + \theta - \frac{\wp_1}{2} - \frac{\Lambda_1}{2(1+\sigma E)} &= 0.44464 > 0,\\
\Lambda_2 + \theta - \frac{\wp_2}{2} - \frac{\Lambda_2}{2(1+\sigma E)} &= 0.32143 > 0,\\
\Lambda_3 + \theta - \frac{\wp_3}{2} - \frac{\Lambda_3}{2(1+\sigma E)} &= 0.18571 > 0,\\
mu - \frac{\Lambda_1 + \Lambda_2 + \Lambda_3}{2(1+\sigma E)} &= 0.11429 > 0.
\end{aligned}$$

Thus, the hypotheses of Theorem 4 are satisfied. The minimum of these four positive numbers

is approximately 0.11429. Consequently, the coefficient in Theorem 5 is $c = 0.2286 > 0$, which guarantees MLS of the unique EP $\mathcal{E}_2^* = (18.2615,\ 1342.2,\ 0.9131,\ 4.5654,\ 12.1743,\ 3.4349)$.

Table 4. Parameter values for the second simulation scenario.

Parameter	Value
π	1000
N	1000
θ_1	0.75
κ	0.005
θ_2	0.04
$\wp_1$	0.025
$\wp_2$	0.1
$\wp_3$	0.2
Λ_1	0.3
Λ_2	0.2
Λ_3	0.1
θ	0.2
σ	0.05
E	50

Figures 4 and 5 display the dynamics obtained with the parameters of Table 4. With this parameter set, the system converges rapidly to the EP. The infertile population $I(t)$ quickly approaches its equilibrium value $I^* = 1342.2$, while the other compartments settle to their (small) positive steady-state values almost immediately, reflecting the very low treatment entry rate. The effect of the FO is still discernible in the early transient phase, but the strong stability overwhelms any memory-induced delay. Figure 5 shows the LF $L(t)$: Its monotonic decay confirms GAS, and the decay rate aligns with the positive coefficient c computed above.

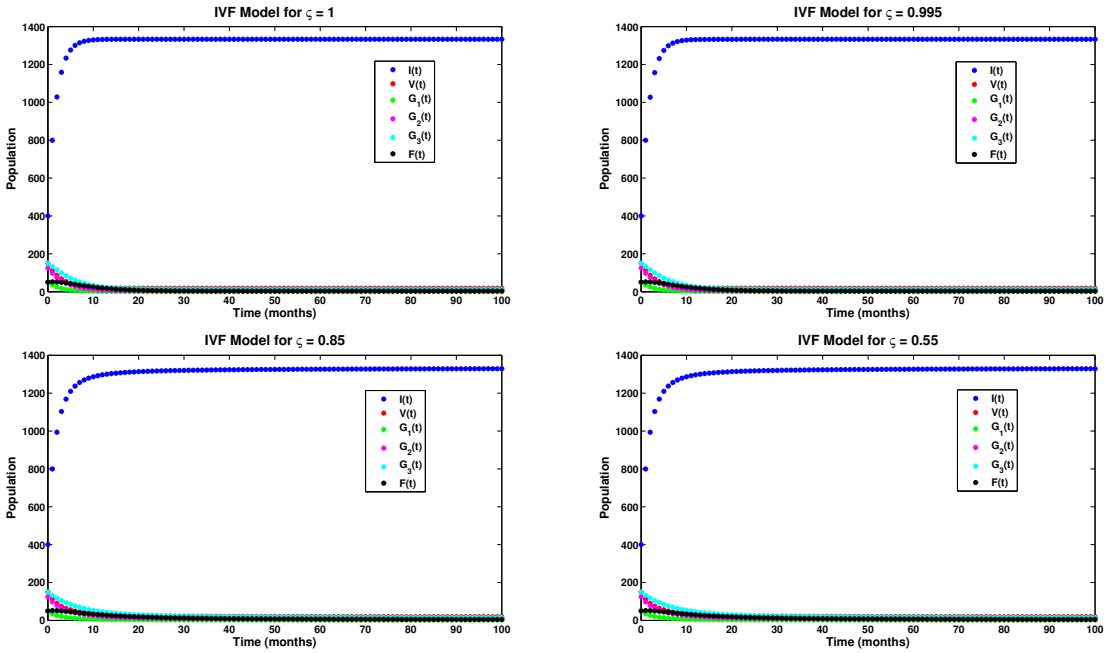

Figure 4. Time evolution of all compartments under the second parameter set for Case 2.

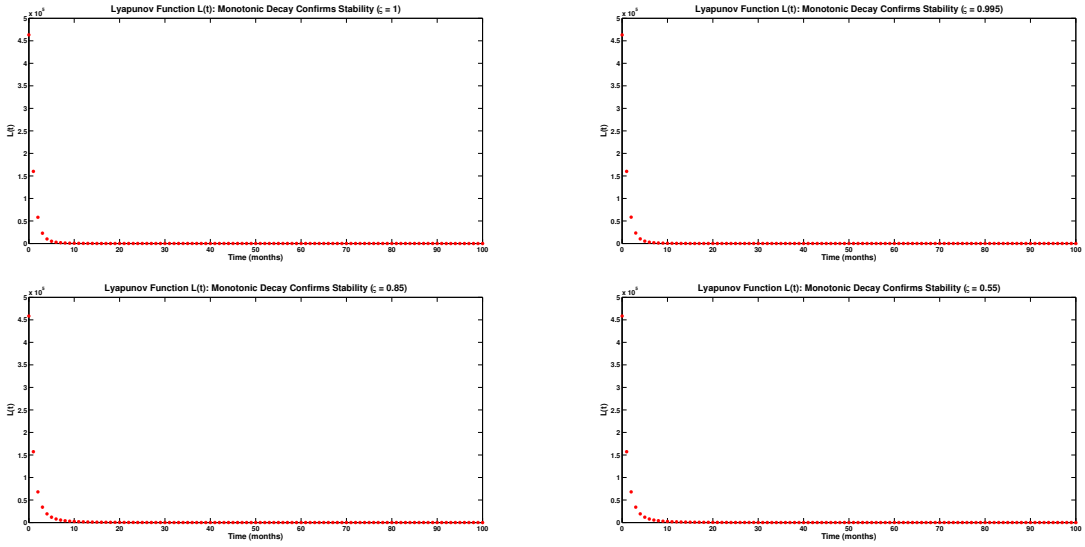

Figure 5. LF $L(t)$ based on the parameter values given in Table 4.

These simulations reinforce the analytical findings that whenever the parameters satisfy the conditions of Theorems 4 and 5, the system converges to the unique EP, and the FO merely modulates the speed of convergence without altering the stability conclusion. The second scenario also illustrates that even with a very low treatment entry rate, the model remains well-behaved and the theoretical guarantees hold.

6. Conclusions

In this work, we have developed and rigorously analyzed a discrete FO mathematical model for IVF dynamics, motivated by real clinical data from the Near East University Hospital IVF clinic. By employing the dual CNFD operator, the model naturally incorporates memory effects and hereditary properties inherent in biological processes such as hormonal regulation, embryo development, and repeated treatment cycles. The discrete formulation aligns seamlessly with the cycle-based nature of clinical data collection, offering a more realistic representation than continuous counterparts. We established fundamental mathematical properties of the model, including the existence and uniqueness of solutions via fixed-point theorems and the non-negativity of state variables through comparison principles. Equilibrium analysis identified a unique positive EP, and we derived sufficient parameter conditions that guarantee GAS and MLS of this equilibrium using a novel Volterra-type discrete LF adapted for fractional difference systems. These conditions provide explicit inequalities that can guide clinicians in optimizing treatment protocols.

Numerical simulations, performed with parameters estimated from clinical data, confirmed the theoretical findings. The results demonstrate that the system always converges to the unique positive equilibrium; the FO modulates the speed of convergence: Lower values introduce delays and stronger memory effects, capturing the protracted nature of IVF cycles more accurately. The LF decay observed in simulations validated the GAS and MLS results, and the model successfully reproduced the expected dynamics under different parameter sets. This study presents the first discrete FO-IVF model validated with real clinical data, offering a mathematically rigorous and practically relevant

tool for understanding the complex dynamics of fertility treatment. By explicitly accounting for the discrete timing of clinical observations and incorporating memory through fractional differences, the model provides deeper insights into time-dependent factors influencing IVF success. In clinical practice, the discrete FO-IVF model offers several concrete applications. First, by calibrating its parameters to clinic-specific data, it can forecast the expected number of positive pregnancy outcomes $F(t)$ and the treatment load $V(t)$ over time, supporting capacity planning and resource allocation. Second, the FO explicitly quantifies the cumulative influence of past cycles on current success; a fitted ς provides a measurable memory index that can guide decisions on cycle spacing and stimulation protocols. Third, the stability conditions derived in Theorems 4 and 5 supply actionable thresholds—for instance, a maximum allowable treatment entry rate or minimum embryo quality rates that help keep the system in a stable, predictable regime. Fourth, by varying the age-related parameters E and σ, the model can compare predicted outcomes for different patient subgroups (younger vs. older, fresh vs. frozen embryos), thereby informing personalised patient counselling. Finally, because the model is mathematically well-posed and globally stable, it establishes a rigorous foundation for future optimal control studies aimed at maximising cumulative live births under financial or medical constraints.

Future work could extend the model to include additional biological complexities, such as age-stratified cohorts, multiple IVF cycles, or resource limitations, and explore optimal control strategies to enhance pregnancy outcomes. The framework established here paves the way for more personalized patient management and improved counseling in reproductive medicine. Despite its strengths, the present model has several limitations that should be acknowledged. First, the average female age E is treated as a constant, whereas in reality age distributions evolve over time and strongly influence embryo quality and implantation success. Second, the model does not incorporate resource or capacity constraints (e.g., limited clinic slots, embryo storage, or financial ceilings), so it cannot capture saturation effects that would bound treatment numbers in a practical setting. Third, the system is purely linear; non-linear feedbacks such as treatment discontinuation after repeated failures, age-dependent success probabilities, or crowding effects are not included. Addressing these limitations offers natural directions for future investigation.

Author contributions

Conceptualization, I.B. and M.M.; methodology, I.B., M.M., and A.O.; software, I.B. and N.A.; validation, I.B., M.M., and A.A.-N.; formal analysis, I.B., M.M., and A.O.; investigation, I.B., M.M., N.A., and A.A.-N.; resources, I.B. and M.M.; data curation, M.M. and I.B.; writing—original draft preparation, I.B., M.M., and A.O.; writing—review and editing, I.B., M.M., A.O., N.A., and A.A.-N.; visualization, I.B. and N.A.; supervision, I.B. and M.M.; project administration, I.B.; funding acquisition, I.B. and A.A.-N. All authors have read and agreed to the published version of the manuscript.

Use of Generative-AI tools declaration

The authors declare they have not used Artificial Intelligence (AI) tools in the creation of this article.

Acknowledgments

This work is supported by Ajman University Internal Research Grant No. [DRGS Ref. 2025-IRG-DRG-3].

Conflict of interest

The authors declare that they have no conflicts of interest.

References

1. B. O. Ibitoye, O. Akadiri, F. O. Ibitoye, O. A. Fasasi, WHO fact sheet on infertility (definition of infertility), published in Global Reproductive Health (2021), *Global Reprod. Health*, **8** (2023), e60. https://doi.org/10.1097/GRH.0000000000000060
2. H. Fertilisation, E. Authority, The current status of IVF: are we putting the needs of the individual first, *eClinicalMedicine*, **65** (2023), 102343. https://doi.org/10.1016/j.eclinm.2023.102343
3. W. M. Hirst, A. Vail, D. R. Brison, S. A. Roberts, Prognostic factors influencing fresh and frozen IVF outcomes: an analysis of the UK national database, *Reprod. BioMed. Online*, **22** (2011), 437–448. https://doi.org/10.1016/j.rbmo.2010.12.008
4. Y. Bentov, J. Schenker, IVF and pregnancy outcomes: the triumphs, challenges, and unanswered questions, *J. Ovarian Res.*, **18** (2025), 228. https://doi.org/10.1186/s13048-025-01692-5
5. A. Al-Nana, I. M. Batiha, Modeling adaptive memory in neural dynamics: a dual nabla fractional-order FitzHugh–Nagumo framework, *Ricerche Mat.*, 2026. https://doi.org/10.1007/s11587-026-01067-y
6. A. K. Alsharidi, M. Qousini, Dynamics and stability of soliton structures for the generalized nonlinear fractional (3 + 1)-dimensional wave model in computational physics, *Fractal Fract.*, **9** (2025), 806. https://doi.org/10.3390/fractalfract9120806
7. N. Hafizi, P. Tulay, Mathematical modeling in reproduction and infertility, In: I. Ozsahin, D. U. Ozsahin, *Applied machine learning and multi-criteria decision-making in healthcare*, Bentham Science Publishers, (2021), 214–234. https://doi.org/10.2174/9781681088716121010014
8. B. Yeolekar, N. Shukla, J. Shukla, M. Yeolekar, S. Patil, P. K. Santra, Optimal control model for IVF treatment in women, *Int. J. Biomath.*, 2024, 2450101. https://doi.org/10.1142/S1793524524501018
9. M. Ghannam, B. Kaymakamzade, M. Farman, K. S. Nisar, F. Aljuaydi, A. Sambas, Investigating the success of IVF with fractional-order model: analysis and case study, *Fractals*, **34** (2026), 2540255. https://doi.org/10.1142/S0218348X25402558
10. A. N. Anber, Z. Dahmani, The Laplace decomposition method for solving nonlinear conformable fractional evolution equations, *Int. J. Open Probl. Comput. Math.*, **17** (2024), 67.
11. I. H. Jebril, Linear and nonlinear control for complete synchronization of fractional-order discrete reaction-diffusion systems, *Int. J. Anal. Appl.*, **24** (2026), 26. https://doi.org/10.28924/2291-8639-24-2026-26

12. P. R. Ashok, S. A. Sayed, A comprehensive review of fractional differential equations and their role in modeling complex dynamical systems, *Int. J. Eng. Sci. Humanit.*, **14** (2024), 71–80.

13. F. M. Atıcı, M. Atıcı, N. Nguyen, T. Zhoroev, G. Koch, A study on discrete and discrete fractional pharmacokinetics-pharmacodynamics models for tumor growth and anti-cancer effects, *Comput. Math. Biophys.*, **7** (2019), 10–24. https://doi.org/10.1515/cmb-2019-0002

14. M. Liu, F. Stella, A. Hommersom, P. J. Lucas, L. Boer, E. Bischoff, A comparison between discrete and continuous time Bayesian networks in learning from clinical time series data with irregularity, *Artif. Intell. Med.*, **95** (2019), 104–117. https://doi.org/10.1016/j.artmed.2018.10.002

15. I. H. Jebril, I. Batiha, A stable and convergent implicit finite difference scheme for variable-order time-fractional convection–diffusion equations, *Int. J. Open Probl. Comput. Math.*, **19** (2026), 73–94.

16. M. Mohammadi, M. Kavousi, T. Madani, P. Amini, A. Ghaheri, Joint modeling of in vitro fertilization outcomes among a population of Iranian infertile couples: a historical cohort study, *Int. J. Fertil. Steril.*, **17** (2023), 306–311. https://doi.org/10.22074/IJFS.2023.562653.1374

17. F. H. Alawad, A. A. Alharbi, K. I. Mayoof, H. M. R. Hawsawi, N. N. Alharthi, R. A. Ahmed, Comparative retrospective analysis of clinical and hormonal profiles in PCOS patients with and without infertility, *J. Adv. Trends Med. Res.*, **1** (2024), 513–518. https://doi.org/10.4103/ATMR.ATMR_21_24

18. L. Sterling, J. Liu, N. Okun, A. Sakhuja, S. Sierra, E. Greenblatt, Pregnancy outcomes in women with polycystic ovary syndrome undergoing in vitro fertilization, *Fertil. Steril.*, **105** (2016), 791–797. https://doi.org/10.1016/j.fertnstert.2015.11.019

19. A. Templeton, J. K. Morris, W. Parslow, Factors that affect outcome of in-vitro fertilisation treatment, *Lancet*, **348** (1996), 1402–1406. https://doi.org/10.1016/S0140-6736(96)05291-9

20. L. G. Cooney, M. D. Sammel, I. Lee, M. A. Clapp, M. Goldsammler, E. Scott, et al., The details matter: personalized prediction of live birth after in vitro fertilization in women with polycystic ovary syndrome, *Fertil. Steril.*, **121** (2024), 1010–1019. https://doi.org/10.1016/j.fertnstert.2024.01.033

21. L. Sterling, J. Liu, N. Okun, A. Sakhuja, S. Sierra, E. Greenblatt, Pregnancy outcomes in women with polycystic ovary syndrome undergoing in vitro fertilization, *Fertil. Steril.*, **105** (2016), 791–797. https://doi.org/10.1016/j.fertnstert.2015.11.019

22. M. Batool, M. Farman, A. Ahmad, K. S. Nisar, Mathematical study of polycystic ovarian syndrome disease including medication treatment mechanism for infertility in women, *AIMS Public Health*, **11** (2023), 19–25. https://doi.org/10.3934/publichealth.2024002

23. Y. Wei, Y. Wei, Y. Chen, Y. Wang, Mittag–Leffler stability of nabla discrete fractional-order dynamic systems, *Nonlinear Dyn.*, **101** (2020), 407–417. https://doi.org/10.1007/s11071-020-05776-3

24. T. Abdeljawad, On delta and nabla Caputo fractional differences and dual identities, *Discrete Dyn. Nat. Soc.*, **2013** (2013), 406910. https://doi.org/10.1155/2013/406910

25. X. Wu, X. Yang, Q. Song, X. Chen, Stability analysis on nabla discrete distributed-order dynamical system, *Fractal Fract.*, **6** (2022), 429. https://doi.org/10.3390/fractalfract6080429

26. Q. Huang, Z. Tu, Discrete-time Mittag–Leffler state estimation for fractional-order quaternion memristive neural networks, *Sci. Rep.*, **15** (2025), 38082. https://doi.org/10.1038/s41598-025-21865-y

27. Y. Wei, Y. Wei, Y. Chen, Y. Wang, Mittag–Leffler stability of nabla discrete fractional-order dynamic systems, *Nonlinear Dyn.*, **101** (2020), 407–417. https://doi.org/10.1007/s11071-020-05776-3

28. A. Al-Nana, I. M. Batiha, Modeling adaptive memory in neural dynamics: a dual nabla fractional-order FitzHugh–Nagumo framework, *Ricerche Mat.*, 2026. https://doi.org/10.1007/s11587-026-01067-y

29. A. Ghaheri, A. Rasekhi, R. O. Samani, E. Hajizadeh, Modeling in vitro fertilization data considering multiple outcomes observed among Iranian infertile women, *Int. J. Fertil. Steril.*, **12** (2018), 27–30. https://doi.org/10.22074/ijfs.2018.5187

30. I. S. Jamadar, K. Kumar, S. A. Khan, A. Khan, M. N. Akhtar, E. A. Bakar, Quantum pressure and memory effects in cancer modeling: a fractional calculus neural network approach, *Results Eng.*, **27** (2025), 106080. https://doi.org/10.1016/j.rineng.2025.106080

31. J. Xu, D. O'Regan, Existence and uniqueness of solutions for a first-order discrete fractional boundary value problem, *RACSAM*, **112** (2018), 1005–1016. https://doi.org/s13398-017-0406-7

32. Z. Lv, C. Wu, D. O'Regan, J. Xu, Solvability of a boundary value problem involving fractional difference equations, *Axioms*, **12** (2023), 650. https://doi.org/10.3390/axioms12070650

33. J. Xu, C. S. Goodrich, Y. Cui, Positive solutions for a system of first-order discrete fractional boundary value problems with semipositone nonlinearities, *RACSAM*, **113** (2019), 1343–1358. https://doi.org/10.1007/s13398-018-0551-7

34. W. Cheng, J. Xu, Y. Cui, Q. Ge, Positive solutions for a class of fractional difference systems with coupled boundary conditions, *Adv. Differ. Equ.*, **2019** (2019), 249. https://doi.org/10.1186/s13662-019-2184-3

35. N. Gopal, J. M. Jonnalagadda, Multiple positive solutions of discrete fractional boundary value problems, *Kragujevac J. Math.*, **50** (2026), 25–38. https://doi.org/10.46793/KgJMat2601.025G

36. I. Bendib, I. Batiha, A. Ouannas, N. Anakira, O. Ogilat, T. Sasa, On general fractional-order discrete-time reaction-diffusion systems: finite time stability and simulations, *Int. J. Rob. Control Syst.*, **5** (2025), 2995–3015. https://doi.org/10.31763/ijrcs.v5i6.1979

37. Y. H. Liang, K. J. Wang, The modified variational principles of the fractal Rosenau–Burgers equation, *Fractals*, 2026. https://doi.org/10.1142/S0218348X26500532

38. Y. Zhang, C. Zhang, K. J. Wang, Qualitative analysis of the fractal complex Hirota-dynamical model for optical fiber communication: variational principle, Hamiltonian and diverse soliton solutions, *Fractals*, **34** (2026), 2650022. https://doi.org/10.1142/S0218348X26500222

39. K. J. Wang, An effective computational approach to the local fractional low-pass electrical transmission lines model, *Alexandria Eng. J.*, **110** (2025), 629–635. https://doi.org/10.1016/j.aej.2024.07.021

Appendix

The choice of the fractional operator is crucial for biological modelling. Continuous fractal–fractional derivatives, such as those proposed in [37, 38], combine a FO with a fractal dimension, enabling the description of processes that are both memory-dependent and scale-dependent. These operators have been applied successfully to heat transfer, fluid dynamics, and epidemic models, where the underlying medium exhibits self-similar or porous structures. Similarly, the generalised fractional derivative discussed in [39] extends classical Caputo and Riemann–Liouville definitions to a wider class of kernels, offering flexibility in capturing anomalous diffusion. In the context of IVF, however, clinical data are recorded at discrete, equally spaced time points (monthly cycle reviews). A continuous operator would require numerical discretisation, which can introduce artificial errors and obscure the exact memory structure implied by the data. The discrete CNFD employed in this work operates directly on the discrete time grid $\mathbb{N}_0$, preserving the exact power-law memory kernel without any approximation of the temporal derivative. Moreover, the nabla (backward) nature of the operator respects causality, a prerequisite for any physiologically meaningful model. The dual CNFD also enjoys the identity $\nabla_a^{-\varsigma}\,{}^{C}\nabla_a^{\varsigma}\mathbf{X}(t) = \mathbf{X}(t)-\mathbf{X}(a)$, which yields an exact Volterra summation representation a property that is not shared by continuous fractal–fractional operators when applied to discrete data. Table A1 summarises the key differences between the operators discussed here, highlighting why the discrete CNFD is the most natural choice for the IVF model.

Table A1. Comparison of fractional operators for biomedical modelling.

Feature	Continuous Caputo derivative	Fractal-fractional derivative [37, 38]	Discrete CNFD (this work)
Time domain	Continuous $\mathbb{R}^+$	Continuous $\mathbb{R}^+$	Discrete $\mathbb{N}_0$
Memory kernel	Power law $(t-s)^{-\varsigma}$	Power law × fractal dimension	Rising factorial $(t-s+1)^{\overline{\varsigma-1}}$
Causality	Yes (Caputo)	Yes	Yes (nabla)
Exact Volterra representation	Integral form (requires discretisation)	Integral form (requires discretisation)	Exact discrete sum
Data alignment	Needs interpolation	Needs interpolation	Direct, cycle-by-cycle
Suitability for IVF	Adequate for theoretical analysis	Suitable for multiscale media	Optimal for discrete clinical records